

Analysis of an Adaptive Strain Estimation Technique in Elastography

S. SRINIVASAN,^{1,2} F. KALLEL,¹ R. SOUCHON³ AND J. OPHIR^{1,3}

¹*The University of Texas Medical School
Department of Radiology
Ultrasonics Laboratory
6431 Fannin St. MSB 2.100
Houston, TX 77030, USA
jonathan.ophir@uth.tmc.edu*

²*University of Houston
Electrical and Computer Engineering Department
4800 Calhoun Rd.
Houston, TX 77204, USA*

³*Inserm
151 Cours Albert Thomas
69424 Lyon Cedex 03, France*

Elastography is based on the estimation of strain due to tissue compression or expansion. Conventional elastography involves computing strain as the gradient of the displacement (time-delay) estimates between gated pre- and postcompression signals. Uniform temporal stretching of the postcompression signals has been used to reduce the echo-signal decorrelation noise. However, a uniform stretch of the entire postcompression signal is not optimal in the presence of strain contrast in the tissue and could result in loss of contrast in the elastogram. This has prompted the use of local adaptive stretching techniques. Several adaptive strain estimation techniques using wavelets, local stretching and iterative strain estimation have been proposed. Yet, a quantitative analysis of the improvement in quality of the strain estimates over conventional strain estimation techniques has not been reported. We propose a two-stage adaptive strain estimation technique and perform a quantitative comparison with the conventional strain estimation techniques in elastography. In this technique, initial displacement and strain estimates using global stretching are computed, filtered and then used to locally shift and stretch the postcompression signal. This is followed by a correlation of the shifted and stretched postcompression signal with the precompression signal to estimate the local displacements and hence the local strains. As proof of principle, this adaptive stretching technique was tested using simulated and experimental data.

KEY WORDS: Adaptive companding; adaptive stretching; contrast-to-noise ratio; cross-correlation; elastography.

INTRODUCTION

Elastography is a technique for imaging the elastic properties of soft tissues and is now well established in the literature.¹⁻⁵ Several strain estimation techniques, like time-domain cross-correlation,⁶ power spectral methods,⁷ Fourier-based speckle phase tracking⁸ and adaptive time domain cross-correlation⁹⁻¹¹ have been developed. The conventionally-used techniques estimate the local axial strain by computing the gradient of the displacements that the tissue elements experience under compression. These displacement estimates are obtained through cross-correlation of the pre- and postcompression rf A-lines that have been temporally stretched.^{12, 13} Stretching the postcompression A-lines improves the correlation between the pre- and postcompression A-lines and reduces the strain noise. However, the

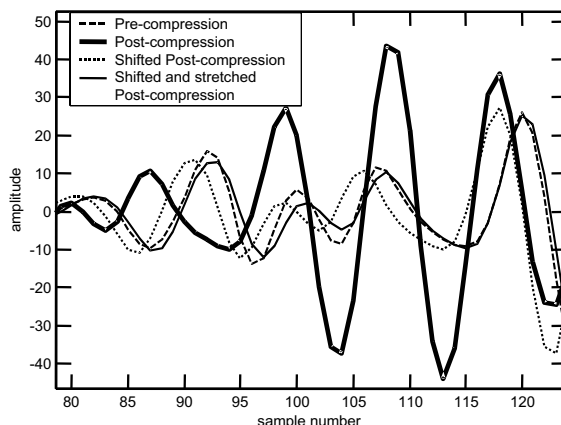


FIG. 1 Illustration of the adaptive stretching technique. Typical rf A-line segments corresponding to (a) precompression, (b) postcompression, (c) shifted postcompression and (d) shifted and stretched postcompression.

use of a constant stretch factor (global stretching) is not optimal in the presence of strain contrast and an accurate prediction of the required stretch factor is difficult in practice. Adaptive time domain cross-correlation techniques overcome these difficulties by estimating strain in localized regions in the tissue. Adaptive estimation of the stretch factor^{9,10} has been used as a direct strain estimator using the maximum correlation coefficient (between the precompression and the stretched postcompression signals) as the criterion. Alternatively, the zero-crossing of the phase of the complex correlation function has been used for an iterative direct strain estimation.¹¹ Yet, a quantitative analysis of the improvement of the quality of the strain estimates over conventional strain estimation techniques, in terms of the contrast-to-noise ratio (CNR_c) has not been reported.

Moreover, the direct strain estimation techniques proposed in references 9 and 10 are computationally intensive and hence might not be suitable for real time strain estimation. Current real time strain estimation techniques^{14,15} are capable of delivering high frame rates using conventional strain estimation schemes.^{6,8} Therefore adaptive strain estimation schemes that could be applicable for real-time strain estimation are preferred to improve the quality of real-time elastograms.

We propose an adaptive technique that utilizes smoothed global displacement and strain estimates to adaptively shift and stretch the postcompression A-line, followed by local strain estimation. This technique differs from the adaptive stretching technique proposed in reference 9 in that this technique involves a two-step strain estimation procedure while the technique proposed in reference 9 is an iterative process. The technique in reference 9 utilizes the maximum value of the correlation coefficient between the precompression and stretched postcompression signals for several values of the stretch factor. Moreover, this technique differs from the 2-D companding scheme proposed in reference 16 in several aspects such as the window size, the presence of a filtering stage in this technique and gradient-strain estimation. A brief description of the technique is provided in the next section and the results are presented in later sections.

TECHNIQUE

The adaptive strain estimation technique involves two stages: (a) estimating the initial displacement and strain using global stretching,¹³ and (b) shifting and stretching the postcomp-

ression segment locally using low-pass-filtered displacement and strain estimate (filtered) respectively, followed by local strain estimation. Figure 1 shows a schematic of the technique applied to a typical rf A-line. For the purpose of illustration, the postcompression A-line is shifted by an amount that is slightly smaller than the local displacement estimate (Fig. 1). The actual shift is not necessarily an integer value and the shifting is done using interpolation techniques.

The strain estimate before the second stage is low-pass-filtered to remove the fluctuations in the displacement and strain estimates that are introduced during the strain estimation process. The use of a least-squares strain estimator¹⁷ provides low-pass-filtered strain estimates directly from the displacement estimate while preserving the edges. Alternatively, filtering (e.g., a moving-average filter) the initial strain estimate (obtained as the gradient of the displacement estimate) could be used. Here, edge-preserving filters that simultaneously perform low-pass filtering¹⁷ (in order to smooth the fluctuations in the strain profile) are preferred. Note that the filtering used in this stage does not affect the spatial resolution of the final elastogram. This is because in the subsequent step, strain is estimated as a gradient of the displacement estimate. The displacement is estimated as the peak of the cross-correlation function between the precompression A-line and the shifted (filtered) and stretched (filtered) postcompression A-line.

The 2-D companding scheme proposed in reference 16 utilizes a similar two-stage strain estimation technique. In their technique, global displacement and strain estimate over several 2-D kernels are first estimated and these estimates are used to estimate strain on a local basis. However, our technique differs from their strain estimation procedure in the following aspects: (a) the window size used in our technique is the same for the global and adaptive strain estimation stages; (b) smoothing the initial strain and displacement estimates before the adaptive strain estimation stage is performed here; and (c) in our technique, strain is computed through a gradient of the displacement estimate rather than through a linear regression scheme.

The performance of this adaptive stretching technique and a comparison with global stretching is made in the next section.

METHODS

As proof of principle, the adaptive stretching technique was tested on simulated and experimental data. A quantitative comparison with global stretching was made with respect to the elastographic contrast-to-noise ratio (CNR_e) and the axial resolution. Note that to study the SNR of elastograms, uniformly elastic phantoms are used. Therefore improvements over global stretching are not expected for SNR studies. The elastographic contrast-to-noise ratio (CNR_e) for a target (t) inside a background (b) has been defined in reference 18 as


$$CNR_e = \frac{2(s_t - s_b)^2}{\sigma_t^2 + \sigma_b^2} \quad (1)$$

where s_t and s_b are the estimated strain values in the target and the background, respectively, and σ_t and σ_b are the standard deviations of the estimated strains.


Simulation studies

For the CNR_e study, simulations involving 2-D models (mechanical and sonographic) were performed using analytical solutions²⁰ on a uniformly elastic phantom with a circular





stiff cylindrical inclusion at the center. The background was simulated as a $40 \times 40 \text{ mm}^2$ region of uniform Young's modulus. The radius of the cylindrical inclusion was fixed at 5 mm and the modulus contrast between the inclusion and the background was varied between 1.5 and 10. Phantoms with four inclusions at given locations were simulated using finite-element techniques (Linear Stress, ALGOR Inc., Pittsburgh, PA). The inclusions along the center of the transducer were five times stiffer than the background and the inclusions located laterally with respect to the center of the transducer were ten times stiffer than the background. The medium was simulated as a set of uniformly-distributed (spatially) scatterers (at a density of 40 scatterers/pulse-width) in both the inclusion and the background. This scatterer density used satisfied the requirement for fully developed speckle.²¹ Monte-Carlo simulations in MATLAB (Mathworks. Inc., Natick, MA) were used to generate pre- and postcompression rf signals for both cases. The speed of sound was assumed to be constant at 1,540 m/s. The impulse-response of the system, i.e., the 2-D point spread function (PSF), was simulated using a Gaussian-modulated cosine pulse (in the axial direction) with a Gaussian intensity profile in the lateral direction at a 5 MHz center frequency, a 50% fractional bandwidth and a -6 dB beam width of 1 mm. The PSF was convolved with the scattering distribution to obtain the precompression rf signal. The postcompression signals were generated after applying a uniform compression of the point scatterers,⁶ and convolving the compressed point scatterer distribution with the original PSF.



For the axial resolution study, a 1-D wedge described in reference 19 was used. This model comprised a stiff inclusion (twice stiffer than the background) at the center of a homogeneous background. The diameter of the inclusion was changed from 0.03 mm to 3 mm in increments of 0.03 mm. The axial resolution was measured using the criterion used in reference 19, i.e., the spatial resolution of the system was defined as the size of the inclusion for which a strain value of at least one pixel (within the inclusion) was midway between the mean strain values corresponding to the background and the inclusion. A strain of 1% was used for the resolution study.

Global correlation was performed by first stretching the postcompression A-line by the applied strain, followed by windowing the pre- and postcompression A-lines and computing the cross-correlation peak between the pre- and postcompression A-lines for each window. A window size (W) of 2 mm and a window overlap of 80% (i.e., a window shift of $0.2W$) were used unless stated otherwise. The time delay for each window was computed as the location of the peak of the cross-correlation function and the incremental strain was estimated as the gradient of the time delay estimates. The incremental strain was added to the global strain (used to stretch the postcompression A-line) to obtain the elastogram. The adaptive correlation described in the previous section was used. The global strain estimate was obtained using the least-squares method¹⁷ (kernel size of at least three pixels) before the adaptive strain estimation. Although this procedure uses the smoothed displacement and strain estimates (to shift and stretch the postcompression rf A-line locally), the final strain estimates are computed as the gradient of the displacement estimates obtained from the correlation of the shifted-and-stretched postcompression A-line segment and the precompression A-line segment. Hence, the least-squares kernel does not result in any filtering of the final strain estimates.

We expect improvements in using adaptive stretching over global stretching at high strains since at low strains the decorrelation due to incorrect stretching is minimal.^{9,13} Hence, an applied strain of 4% was used in the simulations unless stated otherwise. For the 2-D simulations, lateral correction was used to reduce the noise due to lateral motion of the scatterers during compression. The lateral correction was performed through a 2-D correlation between a single precompression A-line and a group of adjacent postcompression A-lines. Such a scheme is similar to the lateral correction technique proposed in reference 22.

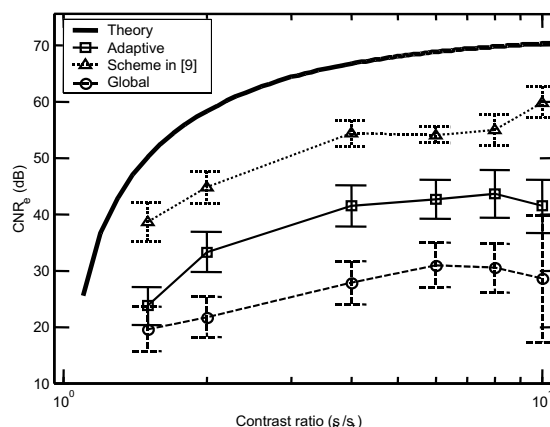


FIG. 2 (a) CNR_c plotted as a function of contrast for both global stretching and adaptive stretching (using a least-squares kernel length of 6 mm). A 10 mm inclusion at the center of a 40×40 mm² background, a 5 MHz (60% fractional bandwidth, 1 mm beamwidth) Gaussian PSF, at an SNR_c of 40 dB, sampled at a frequency of 48 MHz, and a 2 mm window at an overlap of 1.6 mm were used in these simulations.

Experiments

Experiments were performed on a $90 \times 90 \times 90$ mm³ gelatin phantom with a cylindrical inclusion (10 mm diameter at an estimated strain contrast of 2.5 as measured from the elastograms) located at the center of the phantom. A 5 MHz, 50% fractional bandwidth 128 element array transducer and an HDI-1000 ultrasound scanner (Philips -ATL corporation., Bothell, WA) was used to image the phantom. The phantom (prepared using the method described in [23]) was imaged across the cylindrical axis and the rf A-lines were sampled at a frequency of 20 MHz.

RESULTS

Simulation results

Figure 2 shows the CNR_c improvement over global stretching due to adaptive stretching for the 2-D model. A statistical analysis was performed to show that the mean values of the CNR_c of the adaptive stretching and global stretching techniques were statistically distinct from each other (p -values < 0.01 over 50 independent realizations). The improvement in the CNR_c values is significant at higher modulus contrasts. The CNR_c values for the global stretching technique decreases at higher modulus contrasts due to incorrect stretching in the regions corresponding to the inclusion. Figure 2 also shows the CNR_c values due to the adaptive processing scheme in reference 9. Note that the CNR_c values of the scheme proposed in reference 9 is significantly higher than those due to the adaptive scheme proposed in this paper. This is because, the scheme in reference 9 performs stretching by several factor until the best correlation is obtained. However the processing time of that scheme is at least 10 times slower than the adaptive scheme proposed in this paper.

For the four-inclusion phantom (Fig. 3) generated using the finite-element simulation, figure 3b shows the elastogram obtained using global stretching and figure 3c shows the elastogram obtained using adaptive stretching. Here too, the effect of inappropriate stretching reflects as higher noise in the regions corresponding to the inclusions in figure 3b.

The adaptive stretching technique is not expected to result in a loss of spatial resolution. This is because the adaptive strain estimation technique does not involve filtering though the

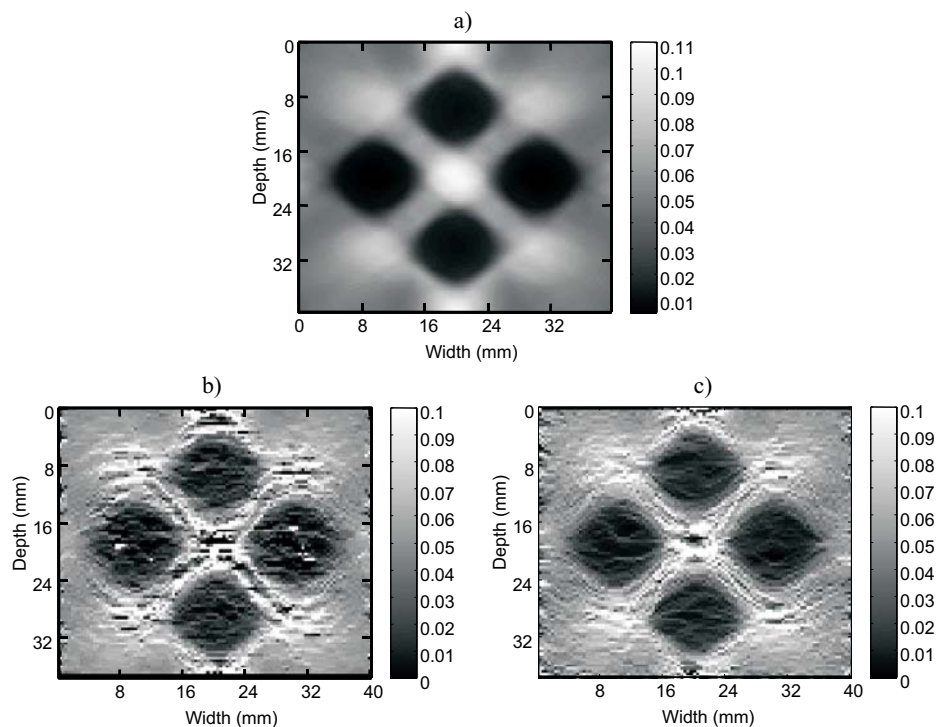


FIG. 3 (a) Axial elastograms generated using ALGOR simulation of four inclusions (10 mm each) in a uniform $40 \times 40 \text{ mm}^2$ background. Axial elastogram obtained using (b) global stretching and (c) adaptive stretching for the displacements generated via the ALGOR simulation. A 5 MHz (60% fractional bandwidth, 1 mm beamwidth) Gaussian PSF, at an SNR_c of 40 dB, sampled at a frequency of 48 MHz and a 2 mm window at an overlap of 1.6 mm were used in these simulations.

initial strain and displacement estimates are filtered. Figure 4a shows the axial resolution plotted as a function of the window length for two different window shifts. Notice a linear degradation of the axial resolution with the window length. These results are consistent with those reported in reference 19. No statistical differences between the resolution values of the adaptive and the global stretching schemes were observed. Similarly, the axial resolution plotted as a function of the fractional window shift is shown in figure 4b. Here too, there were no statistically-significant differences between the adaptive stretching and global stretching schemes.

Experimental results

Figures 5a and 5b show the elastograms of a cross-section of cylindrical inclusion obtained using global and adaptive stretching, respectively. The strip of high strain on the right side of the inclusion is probably due to a crack in the phantom that may also be seen in the sonogram as a hypoechoic region (Fig. 5c). In these figures, a 5×5 pixel 2-D median filter was used to smooth the displacement estimates and the strain was estimated using a 1 mm least-squares kernel on the smoothed displacement estimates.

The strain contrast measured from the elastogram was approximately 2.5. For such a contrast, the CNR_c as a function of strain is shown in figure 6a. Here the CNR_c was computed by taking a rectangular strip of pixels from the background and the inclusion of the strain image. Note that filtering was not used while computing the CNR_c . Ten independent realizations of a multi-compression experiment (20 compressional steps of 0.25% strain for each compres-

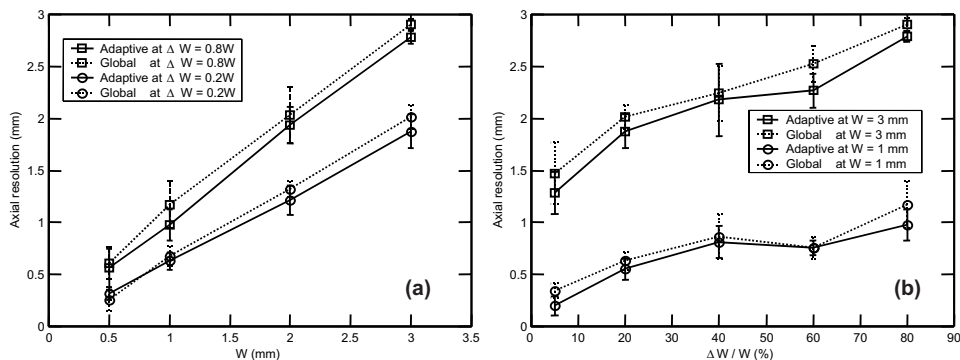


FIG. 4 Axial resolution plotted as a function of (a) window length and (b) window shift. A 5 MHz, 60% fractional bandwidth Gaussian PSF, at an SNR_s of 40 dB, sampled at a frequency of 48 MHz and an applied strain of 1% were used.

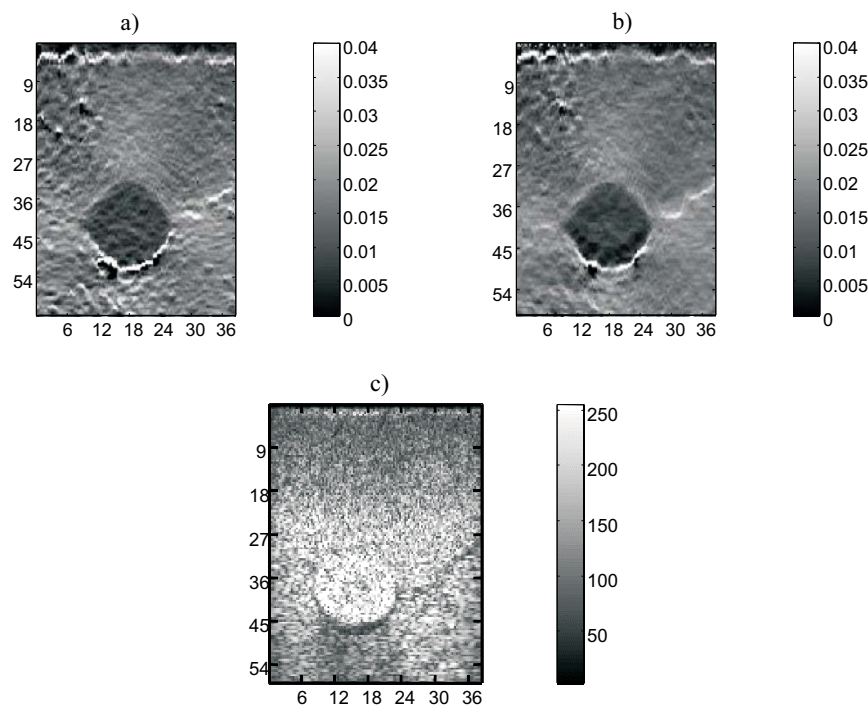


FIG. 5 Axial elastograms obtained using (a) global stretching and (b) adaptive stretching for displacements of a uniformly elastic phantom ($90 \times 90 \times 90 \text{ mm}^3$) with a cylindrical inclusion (14 mm diameter) located 40 mm below the compressor. The phantom was compressed 2% axially and imaged to a depth of 57 mm with a 5 MHz, 60% fractional bandwidth array transducer, sampled at a frequency of 20 Mhz. A 2 mm window at an overlap of 1.6 mm was used. (c) Sonogram corresponding to the elastograms in (a) and (b).

sion step) were used to compute the statistics. The stress-strain relationships in tissues and gelatin phantoms are linear up to a strain of around 3%²⁴ and, hence, the contrast is not expected to change significantly in this strain range. The improvement in CNR_e is clear from figure 6a. It is to be noted that the CNR_e values are significantly lower than those corresponding to the simulations (at the same contrast) due to several possible reasons. These include nonuniform compression, frequency-dependent attenuation, lower SNR_s , out-of-plane mo-

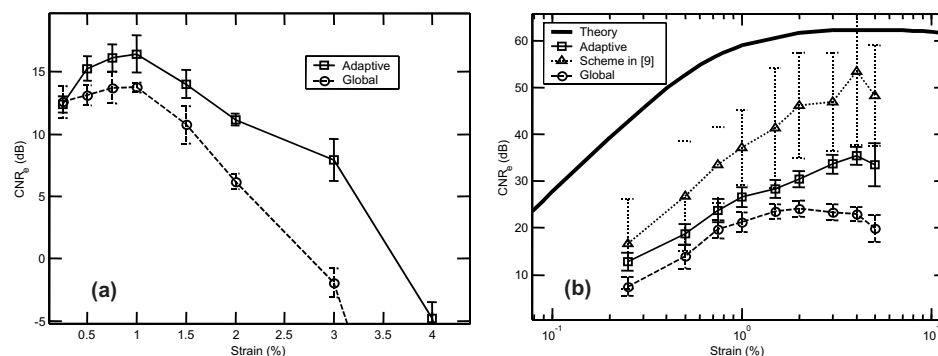


FIG. 6 (a) CNR_e plotted as a function of strain for both global stretching and adaptive stretching (using a least-squares kernel length of 6 mm) for experiments and (b) comparison of simulations and experimental results for adaptive stretching. A uniformly elastic phantom ($90 \times 90 \times 90 \text{ mm}^3$) with a circular inclusion (14 mm diameter) located 40 mm below the compressor plate was used and imaged to a depth of 57 mm with a 5 MHz, 60% fractional bandwidth array transducer, sampled at a frequency of 20 Mhz. A 2 mm window at an overlap of 1.6 mm was used.

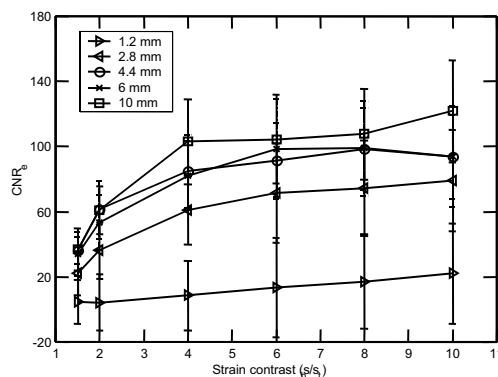


FIG. 7 CNR_e plotted as a function of contrast for the adaptive stretching technique for several least-squares kernel lengths. A 10 mm inclusion at the center of a $40 \times 40 \text{ mm}^2$ background and a 5 MHz, 60% fractional bandwidth gaussian PSF, at an SNR_e of 40 dB, sampled at a frequency of 48 MHz were used. A 2 mm window at an overlap of 1.6 mm was used in these simulations

tion and nonuniform strain distribution within the inclusion and in the background. For the same reasons, the experimental values of CNR_e decrease significantly at strains greater than 1%. The CNR_e values due to global and adaptive stretching in simulations of a 10 mm inclusion at a modulus contrast of 2.5 are shown in figure 6b. For strains larger than 2%, the CNR_e decreases with strain for the global stretching because the difference in the displacements inside the inclusion and around the inclusion increases with the strain. The improvement due to adaptive stretching over global stretching is higher in the simulations than in the experiments due to the effects of undesired decorrelation in experiments. Figure 6b also shows the CNR_e values due to the scheme in reference 9 to facilitate a fair comparison of our adaptive scheme with a ‘true’ adaptive stretching scheme.

DISCUSSION

Our adaptive strain estimation technique involves two stages, unlike the adaptive technique proposed in reference 9, which is based on testing several stretch factors until the highest correlation coefficient occurs. Hence, our technique could result in significantly smaller

processing times. For example, the processing time of our scheme is of the order of $2kM\log_2 N$, while the processing time for the technique in reference 9 is $mkM\log_2 N$, where N is the number of samples in the correlation window, k is the number of windows in the elastogram and m is an integer greater than 10.⁹ Yet, the adaptive scheme in reference 9 is based on obtaining the largest correlation between the pre- and postcompression signals and, therefore, produces less noisy elastograms with higher CNR_e values than our technique (Fig. 2).

Low-pass-filtering the initial global strain estimate is necessary to improve the performance of our adaptive strain estimation technique. This is because filtering removes the fluctuations in the displacement and strain estimates that are introduced during the strain estimation process. These fluctuations could be due to inappropriate stretching (in the presence of nonhomogenous phantoms) and random errors in strain estimation. We use a least-squares estimator to estimate the initial value of strain. Alternatively, a moving average filter was tried. We found that the least-squares kernel preserved the edges better than the moving average filter.¹⁷ Other filtering techniques that involve low-pass filtering to smooth the strain estimates such as median filtering were tried. However, no significant improvements were observed.

The size of the least-squares kernel that results in the highest CNR_e depends on the size of the inclusion. If the kernel size is larger than the inclusion, the initial strain estimate for stretching the postcompression signal is different from the actual value in the regions close to the inclusion. This results in strain estimates with higher variance around the areas of the inclusion and hence poor CNR_e . The best performance is for kernel sizes that are comparable to inclusion sizes. 1-D simulations were performed to demonstrate the effect of the kernel size on the CNR_e for a 10 mm inclusion and the results are summarized in figure 7. It can be seen from the figure that the kernel size (for high values of CNR_e) corresponds to the inclusion size.

The adaptive stretching technique discussed in this paper is not expected to result in a loss of spatial resolution. This is because the adaptive strain estimation technique does not involve filtering though the initial strain and displacement estimates are smoothed. A systematic comparison of the axial resolution of this scheme with the scheme in reference 9 is beyond the scope of this work.

CONCLUSION

A quantitative analysis of the improvement in the elastographic contrast-to-noise ratio using adaptive stretching over conventional (global stretching) strain estimation techniques has been performed using simulations and phantom experiments. An adaptive stretching technique that involves the use of global and local stretching has been developed for elastography. This technique was found to produce significant improvements in the contrast-to-noise ratio over global stretching techniques, without affecting the axial resolution, at large values of modulus contrasts and strains.

ACKNOWLEDGEMENTS

This work was supported by the National Cancer Institute program project P01-CA64597 awarded to the University of Texas Medical School, Houston. The authors would like to thank R. Righetti for her helpful comments on the paper.

REFERENCES

1. Ophir, J., Cespedes, I., Ponnekanti, H., Yazdi, Y., and Li, X., Elastography: a quantitative method for imaging the elasticity of biological tissues, *Ultrasonic Imaging* 13, 111-134 (1991).
2. Ophir, J., Cespedes, I., Garra, B., Ponnekanti, H., Huang, Y. and Maklad, N., Elastography: ultrasonic imaging of tissue strain and elastic modulus in vivo, *Eur. J. Ultrasound*, 49-70 (1996).
3. Ophir, J., Alam, K.S., Garra, B., Kallel, F., Konofagou, E.E., Krouskop, T.A. and Varghese T. Elastography: Ultrasonic estimation and imaging of the elastic properties of tissues, *Proc. Inst. Mech. Eng. Part HJ, Engineering in Medicine* 213, 203-233 (1999).
4. Emalianov, S.Y., Lubinski, M.A., Weitzel, W.F., Wiggins, R.C., Skovoroda, A.R. and O'Donnell, M., Elasticity imaging for early detection of renal pathology, *Ultrasound Med. Biol.* 21, 871-883 (1995).
5. Gao, L., Parker, K.J., Lerner, R.M., Levinson, S.F., Imaging of the elastic properties of tissue: a review, *Ultrasound Med. Biol.* 22, 959-977 (1996).
6. Cespedes, I. Elastography: imaging of biological tissue elasticity, *Ph.D. Dissertation*, University of Houston, (1993).
7. Konofagou, E.E., Varghese, T., Ophir, J. and Alam, S.K., Power spectral strain estimators in elastography, *Ultrasound Med. Biol.* 25, 1115-1129 (1999).
8. O'Donnell, M., Skovoroda, A.R. and Shapo, B.M., Measurement of arterial wall motion using Fourier based speckle tracking algorithms, in *Proc. 1991 IEEE Ultras. Symp.* 2, pp. 1101-1104 (1991).
9. Alam, S.K., Ophir, J. and Konofagou, E., An adaptive strain estimator for elastography, *IEEE Trans Ultrason. Ferroelec. Freq. Cont.* 45, 461-472 (1998).
10. Bilgen, M., Wavelet transform-based strain estimator for elastography, *IEEE Trans Ultrason. Ferroelec. Freq. Cont.* 46, 1407-1415 (1999).
11. Brusseau, E., Perrey, C., Delachartre, P., Vogt, M., Vray, D., Ermert, E., Axial strain imaging using a local estimation of the scaling factor from rf ultrasound signals, *Ultrasonic Imaging* 22, 95-107 (2000).
12. Cespedes, I., Ophir, J., Reduction of image noise in elastography, *Ultrasonic Imaging* 15, 89-102 (1993).
13. Varghese, T. and Ophir, J., Enhancement of echo-signal correlation in elastography using temporal stretching, *IEEE Trans. Ultrason. Ferroelec. Freq. Cont.* 44, 173-180 (1997).
14. Pesavento A., Perry C., Krueger M. and Emert H., A time efficient, and accurate strain estimation concept for ultrasonic elastography using iterative phase zero estimation, *IEEE Trans. Ultrason. Ferroelec. Freq. Cont.* 46, 1057-1067 (1999).
15. Hall J. T., Zhu Y., Spalding C.S. and Cook L.T., In-vivo results of real-time freehand elasticity imaging, in *Proc. IEEE. Ultrason. Symposium*, p. 1653 (2001).
16. Chaturvedi, P., Insana, M.F. and Hall, T.J., 2-D companding for noise reduction in strain imaging, *IEEE Trans Ultrason. Ferroelec. Freq. Cont.* 45, 179-191 (1998).
17. Kallel, F. and Ophir, J., A least-squares strain estimator for elastography, *Ultrasonic Imaging* 19, 195-208 (1997).
18. Bilgen, M., and Insana, M.F., Target detectability in acoustic elastography, *IEEE Trans. Ultrason. Ferroelec. Freq. Cont.* 46, 1128-1133 (1999).
19. Alam, S.K., Ophir, J. and Konofagou, E., Axial resolution criteria in elastography: an empirical study, *IEEE Trans Ultrason. Ferroelec. Freq. Cont.* 45, 461-472 (2000).
20. Kallel, F., Bertrand, M. and Ophir, J., Fundamental limitations on the contrast-transfer efficiency in elastography: an analytic study, *Ultrasound Med. Biol.* 22, 463-470 (1996).
21. Zagebski, J.A., Chen, J.F., Dong, F. and Wilson, T., Intervening attenuation affects first-order statistical properties of ultrasound echo signals, *IEEE Trans. Ultrason. Ferroelec. Freq. Cont.* 46, 35-40 (1999).
22. Konofagou, E.E. and Ophir, J., A new elastographic method for strain estimation and imaging of lateral displacements, lateral strains, corrected axial strains and poisson's ratios in tissues, *Ultrasound Med. Biol.* 24, 1183-1199 (1998).
23. Kallel, F., Prihoda, C.D. and Ophir, J., Contrast-transfer efficiency for continuously varying tissue moduli: simulation and phantom validation, *Ultrasound Med. Biol.* 27, 1115-1125 (2001).
24. Mridha, M. and Odman, S., Characterization of subcutaneous edema by mechanical impedance measurements, *J. Invest. Dermatology* 5, 575-578 (1985).